AFRL-RY-WP-TR-2011-1262

RADIO FREQUENCY AND OPTICAL METAMATERIALS

John S. Derov and Alvin D. Drehman

IR Sensor Technology Branch
Electromagnetics Technology Division

Everett E. Crisman

University of Rhode Island

Beverly Turchinetz

Analog Technologies, Inc.

OCTOBER 2011
Interim Report

AIR FORCE RESEARCH LABORATORY
SENSORS DIRECTORATE
WRIGHT-PATTERSON AIR FORCE BASE, OH 45433-7320
AIR FORCE MATERIEL COMMAND
UNITED STATES AIR FORCE

NOTICE AND SIGNATURE PAGE

Using Government drawings, specifications, or other data included in this document for any purpose other than Government procurement does not in any way obligate the U.S. Government. The fact that the Government formulated or supplied the drawings, specifications, or other data does not license the holder or any other person or corporation; or convey any rights or permission to manufacture, use, or sell any patented invention that may relate to them.

This report was cleared for public release by the Wright-Patterson Public Affairs Office and is available to the general public, including foreign nationals. Copies may be obtained from the Defense Technical Information Center (DTIC) (http://www.dtic.mil).

AFRL-RY-WP-TR-2011-1262 HAS BEEN REVIEWED AND IS APPROVED FOR PUBLICATION IN ACCORDANCE WITH THE ASSIGNED DISTRIBUTION STATEMENT.

*//Signature//

JOHN DEROV, Work Unit Manager
IR Sensor Technology Branch
Electromagnetics Technology Division

//Signature//

MARK SCHMITT, Chief
IR Sensor Technology Branch
Electromagnetics Technology Division

//Signature//

WILLIAM MOORE, Division Chief
Electromagnetics Technology Division
Sensors Directorate

This report is published in the interest of scientific and technical information exchange, and its publication does not constitute the Government's approval or disapproval of its ideas or findings.

*Disseminated copies will show "//signature//" stamped or typed above the signature blocks.

REPORT DOCUMENTATION PAGE

Form Approved
OMB No. 0704-0188

1. REPORT DATE *(DD-MM-YY)*	2. REPORT TYPE	3. DATES COVERED *(From - To)*
October 2011	Interim	01 October 2009 – 30 September 2011

4. TITLE AND SUBTITLE

RADIO FREQUENCY AND OPTICAL METAMATERIALS

5a. CONTRACT NUMBER
IN-HOUSE

5b. GRANT NUMBER

5c. PROGRAM ELEMENT NUMBER
61102F

6. AUTHOR(S)

John S. Derov and Alvin D. Drehman (Electromagnetics Technology Division, IR Sensor Technology Branch (AFRL/RYHI))
Everett E. Crisman (University of Rhode Island)
Beverly Turchinetz (Analog Technologies, Inc.)

5d. PROJECT NUMBER
2305

5e. TASK NUMBER
HA

5f. WORK UNIT NUMBER
2305HA10

7. PERFORMING ORGANIZATION NAME(S) AND ADDRESS(ES)

Electromagnetics Technology Division
IR Sensor Technology Branch (AFRL/RYHI)
Air Force Research Laboratory, Sensors Directorate
Wright-Patterson Air Force Base, OH 45433-7320
Air Force Materiel Command, United States Air Force

University of Rhode Island
Chem. Eng. Crawford Hall
Kingston, RI 02881

Analog Technologies, Inc.
44 Manning Road, Suite 200
Billerica, MA 01821

8. PERFORMING ORGANIZATION REPORT NUMBER
AFRL-RY-WP-TR-2011-1262

9. SPONSORING/MONITORING AGENCY NAME(S) AND ADDRESS(ES)

Air Force Research Laboratory
Sensors Directorate
Wright-Patterson Air Force Base, OH 45433-7320
Air Force Materiel Command
United States Air Force

10. SPONSORING/MONITORING AGENCY ACRONYM(S)
AFRL/RYHI

11. SPONSORING/MONITORING AGENCY REPORT NUMBER(S)
AFRL-RY-WP-TR-2011-1262

12. DISTRIBUTION/AVAILABILITY STATEMENT
Approved for public release; distribution unlimited.

13. SUPPLEMENTARY NOTES
PAO Case Number: 88ABW 2011-6268, cleared 02 December 2011. Report contains color.

14. ABSTRACT

This research encompassed the study of radio frequency (RF) and optical metamaterials. The RF study of metamaterials focuses on the polarization behavior of split-ring-resonators (SRR), wire-post (WP) elements, and the spatially dispersive behavior of the SRR-WP elements. The optical study of metamaterials consisted of using the nano -dot and -particle media for their electric and magnetic plasmon behavior.

15. SUBJECT TERMS
negative refractive index, left-handed materials, double negative, metamaterials, plasmonics

16. SECURITY CLASSIFICATION OF:			17. LIMITATION OF ABSTRACT:	18. NUMBER OF PAGES	19a. NAME OF RESPONSIBLE PERSON (Monitor)
a. REPORT	b. ABSTRACT	c. THIS PAGE			John Derov
Unclassified	Unclassified	Unclassified	SAR	24	19b. TELEPHONE NUMBER *(Include Area Code)* N/A

Table of Contents

Section **Page**

List of Figures

Figure **Page**

1.0 Summary

The study of radio frequency (RF) metamaterials focuses on the polarization behavior of split-ring-resonator (SRR) and wire post (WP) elements and the spatially dispersive behavior of the SRR-WP elements. The SRR elements used in this study were two identical SRRs parallel to each other with their gaps in opposing orientations. The WP was placed between the rings with geometrical symmetry. The metal SRRs and WPs were separated by 10 millimeter thick dielectric with a relative permittivity of 2.2. The polarization behavior of the SRR-WP unit cell was simulated SRRs in the SRR-WP unit cells rotated between 0° and 170° about the center axis of the rings, using Asys's high frequency structure simulator (HFSS). The results showed how the rotation of the gap orientation relative to the incident linearly polarized electric field shifts the resonant frequency of the SRR-WP element.

The spatial behavior was studied by changing the SRR-WP unit cell's geometrical parameters such as the SRR-diameter and WP post width. The simulated results showed the shift in resonant frequency and the change in effective permittivity and permeability with the variation of the SRRs geometrical parameters. By changing the geometrical parameters, coupling between neighboring SRRs and coupling between the WP and SRRs can be observed, thus affecting the relative permittivity and permeability of the metamaterial medium.

The study of the optical metamaterials consisted of using the nano -dot and -particle media for their electric and magnetic plasmon behavior. A layered medium of random nanodots was fabricated and characterized for its plasmon behavior. No plasmon behavior was observed in the random nanodot medium, but polariton behavior was observed by probing the medium with TM mode electromagnetic radiation. Ordered arrays of nanoparticle and nanoparticle clusters were also fabricated. The nanoparticle clusters consisted of four nanoparticles in the form of a ring and were fabricated to generate magnetic plasmon behavior in the medium. Simulations showed strong magnetic plasmon behavior in the 1.5 to 3 μm wavelength range with secondary weaker magnetic plasmon behavior in the 650 to 850 nm visible regime.

2.0 Radio Frequency Metamaterials

The RF research focused on balanced SRR and WP elements. The unit cells for the negative refractive index media [1] that were fabricated and characterized are shown in Figure 1. The unit cell consists of balanced SRRs [2] with the WP centered and between the SRRs. The balanced SRRs have 2 rings of the same diameter parallel to each other with their gaps oriented opposite as shown in Figure 1. When the SRRs are at resonance the current produce in each respective SRR is in the opposite direction, balancing the current distribution and generating a symmetric the field around the SRRs. Figure 1 also shows the angular reference for orientation of the SRR gaps used throughout this study for the 0° and 90° orientation of the SRR gaps. This also defines a clockwise direction of rotation from 0° to 90° for the SRR gaps.

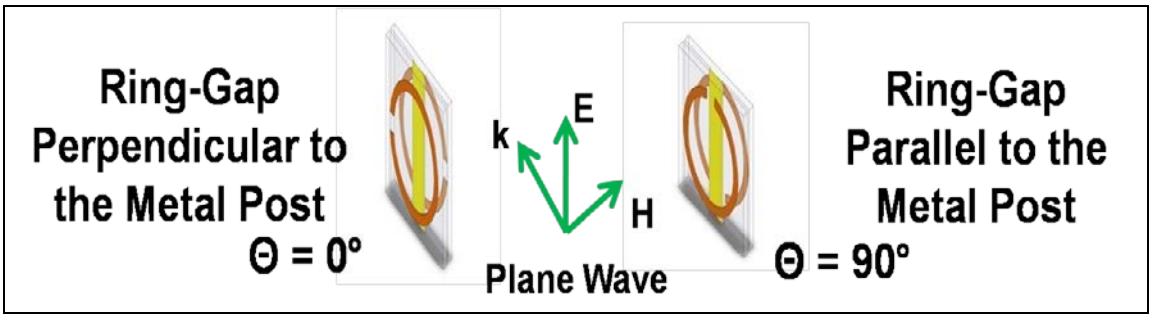

Figure 1. Balanced SRRs.
Two SRRs of the Same Diameter Parallel to Each Other with Their Gaps Oriented Opposite Each Other. The Reference Angles for 0° and 90° Is Also Shown fFor The Srr Gaps.

The measured frequency response and the refractive index as determined by Snell's law [3] are shown in Figure 2 for each of the configurations. Since the orientation of the electric field of the propagating wave is parallel to the WP as shown in Figure 1, it is the effect of the orientation of the electric field relative to the SRR gaps that is observed in the frequency response of the balanced SRR-WP media (Figure 2).

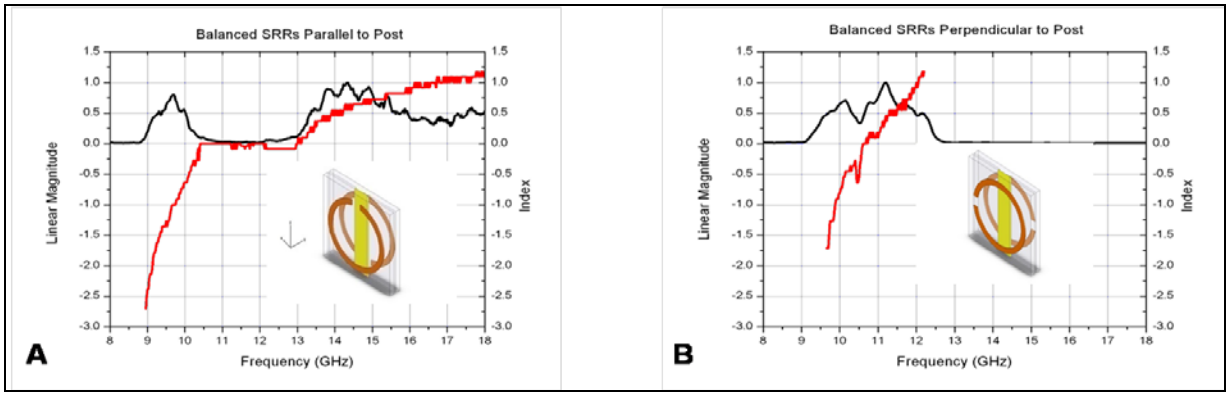

Figure 2. Measured Frequency Response and Refractive Index for the SRR-WP Media. In the Two Ring Orientations (0°, 90°).

Figure 3 shows that the frequency response of the SRRs is sensitive to the direction of the incident electric field relative to the gap of the SRRs. To investigate this further we ran simulations of the SRR-WP unit cell rotating the SRRs form 0° to 170° in 10° increments. In Figure 3 the frequency response of the normalized transmission is shown for gaps oriented at 10° and 170°. The results in Figure 3 show that the frequency response for the SRR gaps at 10° and 170° is almost identical and the rotation of the SRRs gaps is symmetric about 90°.

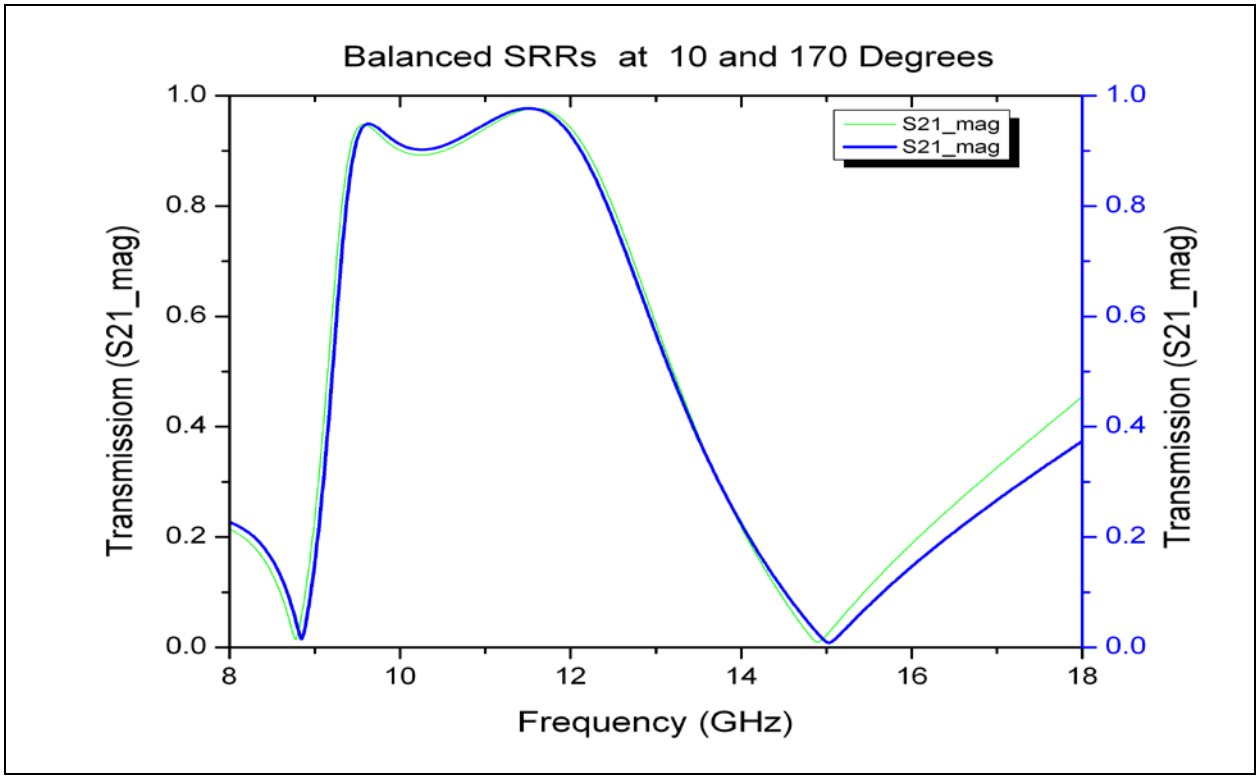

Figure 3. Frequency Response for the Normalized Transmission of the Unit Cell for the SRR Gaps. Oriented at 10° and 170° At Symmetric Orientations About 90°.

Figure 4 shows the results of the simulated frequency response of the normalized transmission through the unit cell at different gap angles 0°, 30°, 60°, and 90°. In Figure 4 it can be seen that the resonance for the unit cell moves from approximately 10 to 9 Giga-Hertz (GHz), while the other resonance moves from approximately 12 to 15 GHz. The simulated response of the unit cell at 0° and 90° is similar to the measured response of the media at 0° and 90°. Figure 4 also shows that the resonance of the SRRs is sensitive to the orientation of the SRRs gaps relative to the electric field of the incident wave. Thus, a linear polarized wave will respond differently in the medium depending on the orientation of the electric field of the incident wave to the gaps of the SRRs.

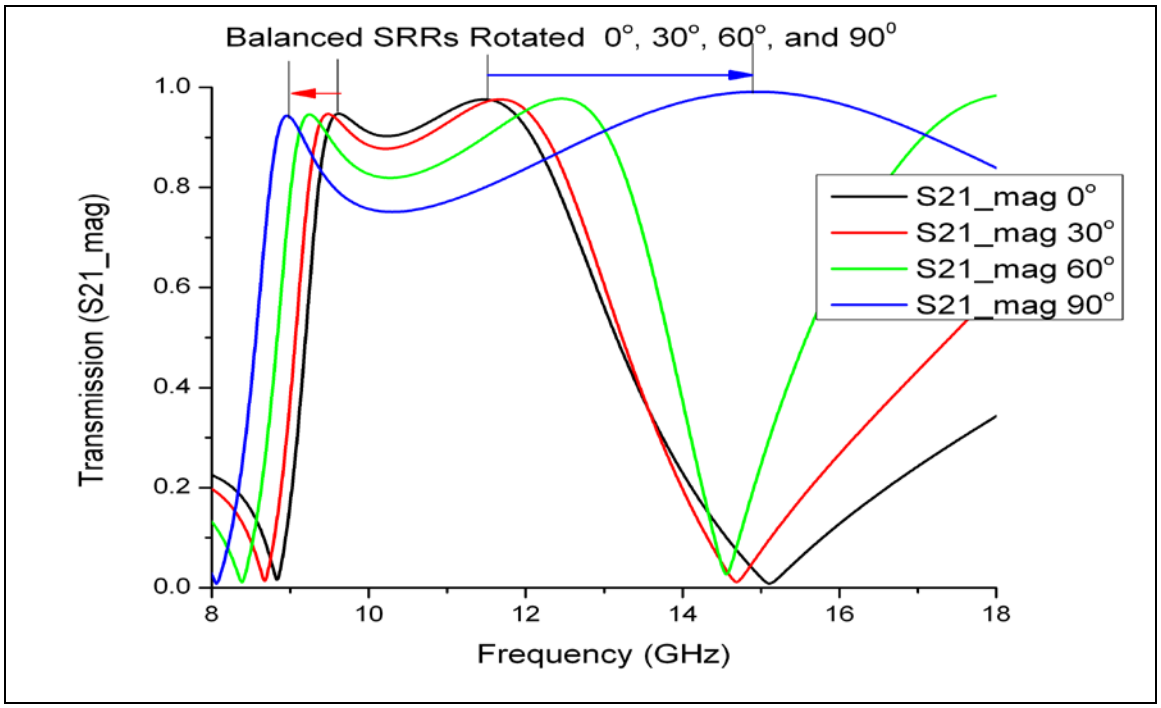

Figure 4. Frequency Response for the Normalized Transmission of the SRR-WP Unit Cell. With the SRR Gaps at 0°, 30°, 60°, and 90°.

To understand what is going on in the media we need to look at how the permittivity (ε) and permeability (μ) is affected by the spatial change. The permeability for the unit cell with the SRR gaps at 0° and 90° is shown in Figure 5.

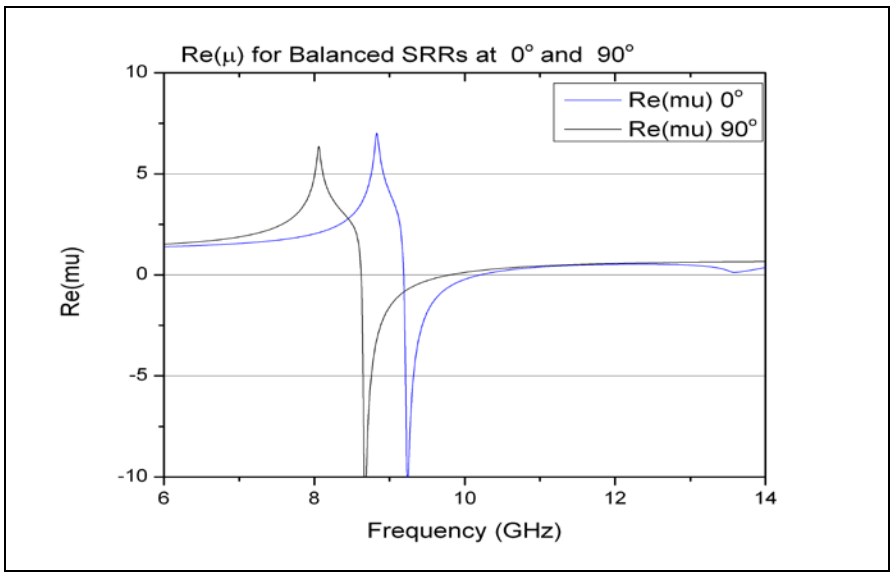

Figure 5. Re(μ) for the Balanced SRR-WP at 0° and 90°.
(The Non-Lorentzian Line is Most Evident for μ Between 6 and 8.5 GHz when the SRR Gaps are at 90°).

The line shape for the permeability is not as Lorentzian shaped as one would expect. As the gap of the SRR is rotated, the line shape of the μ approaches a Lorentzian shape. Since the line shape of μ shows the effect of changing the electric orientation with respect to the SRR, we used the line shape of μ determined from the simulated scattering parameters of the unit cell to determine the effect of the geometrical parameters of the SRRs and WPs.

We started by changing the diameter of the SRR in the unit cell. The outer diameter of the SRR was change from 3.8 to 2.8 mm holding the SRR gaps at 0° and the size of unit cell constant at 4.06 mm. Figure 6 shows the frequency response of the Re(μ)and Re(ε) for these conditions. As the outer diameter of the SRR changes from 3.8 to 2.8 mm the resonant frequency moves from lower to higher frequency. This is expected as the resonator line length goes from longer to shorter. It is the line shape of μ in Figure 6 that shows how the spatial dispersion is changing as the diameter of the SRRs is changed. As the diameter of the SRR is reduced in size, the line shape of μ is still asymmetric, but the line shape of μ is moving toward a Lorentzian line shape. The smallest SRR diameter at 2.8 mm unit cell is the least affect by the spatial dispersion.

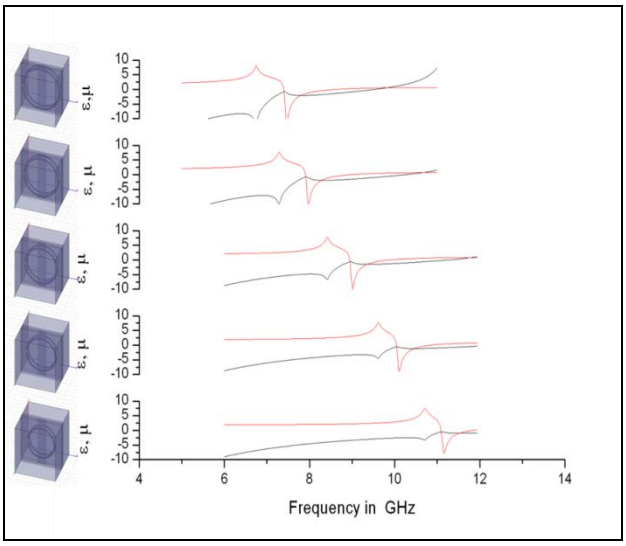

Figure 6. Frequency Response for Re(ε) and Re(μ).
The Diameter of the SRRwas Changed from 3.8 to 2.8 mm.
(The line shape of μ becomes more Lorentzian line like).

Since the line shape of μ was still asymmetric, the orientation of gaps and diameter of the SRR was held constant and the width of the WP was varied from 0.75 to 0.25 mm. Since the WP shape was varied, both ε and μare affected. Figure 7 shows the frequency response of ε and μ. The line shape of μ becomes a symmetric Lorentzian shape at the resonant frequency when the width of the post is reduced to 0.25 mm.

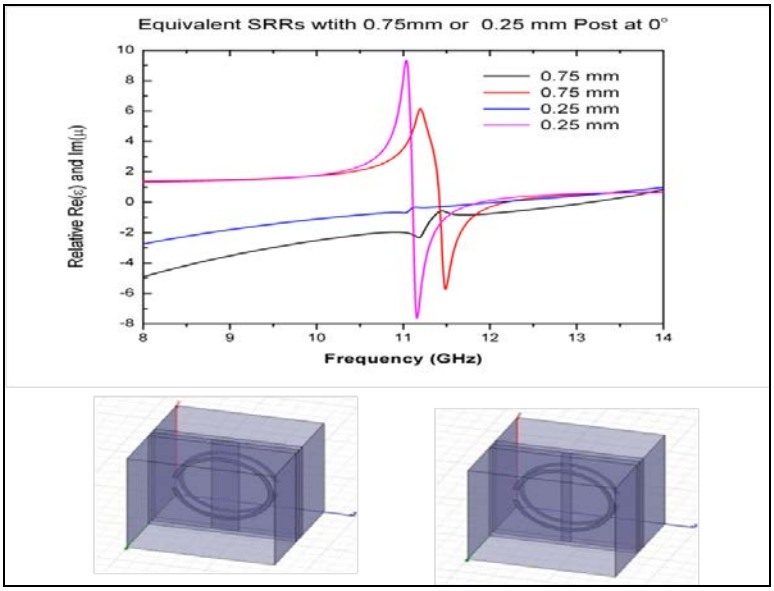

Figure 7. Frequency Response of ε and μ for a SRRWP Unit Cell.
The Diameter of the SRRs at 2.8 mm, the SRR Gaps at 0°, and the Size of the Unit Cell at 4.06 mm.
(The Line Shape for μ Take on the Expected Lorentzian Line Shape when the WP is 0.25mm Wide).

Since the line shape of μ was affected by changing the width of the post, coupling between the WP and the SRRs is evident. The result indicates the coupling between neighboring SRRs and the SRRs and between the WP is important to produce a negative index of refraction.

3.0 Optical Metamaterials

The optical metamaterials research focused on the study of electric and magnetic plasmon elements to produce a medium with simultaneous negative ε and μ. Electric plasmon behavior for nanoparticles has been described as resonant electric dipole moments that allows a wave to propagate through a medium of nanoparticles and is considered to be analogous to a longitudinal wave produced by a resonance in plasma. The magnetic plasmon is caused by a cluster of nanoparticles that produces a magnetic dipole moment at a resonant frequency of the nanoparticle cluster. To produce a medium with either an electric or magnetic plasmon behavior two fabrication methods were used: 1) random nanoparticles were fabricated by depositing thin metal films of approximately 50nm in thickness on Aluminum Oxide (Al_2O_3) substrate. The gold films were annealed at approximately 500° C to form nanodots on the surface of the substrate. 2) Ebeam lithography was used to pattern an array of nanocylinders or arrays of nanocylinder clusters.

To characterize the nanodot media, ATR was used. Figure 8 shows a diagram of the ATR setup for probing materials with transverse electric (TE) and magnetic waves (TM). In the diagram an air gap exists between the prism and the test medium so that total-reflection will occur above the critical angle for the cylindrical-lens-air-interface. When α is greater than or equal to the critical angle, total-reflection occurs and an evanescent TE or TM surface wave is produced along the cylindrical-lens-air interface. The evanescent TE or TM wave can couple to a plasmon-polariton at the air-nanoparticle-medium interface shown in Figure 8.

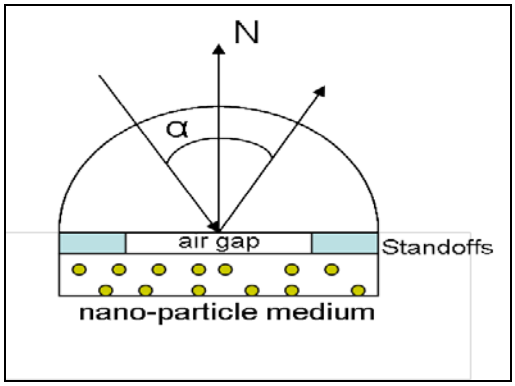

Figure 8. Diagram of a Prism-Spacer-Metal (Otto) Configuration.

To test our ATR setup, we characterized a thin gold film for its surface plasmon resonance. The intensity of the reflectivity was measured as a function of angle for the light incident at the air-cylindrical-lens interface. Figure 9 shows results for the continuous gold metal film from the ATR measurements. The measurements show that a surface plasmon resonance occurs for the p-polarized TM wave above the critical angle, but no resonance is observed for the s-polarized TE wave. The coupling efficiency of the TM wave to the plasmon resonance can be controlled by adjusting the thickness of the air gap. In Figure 9 the dip in the reflectivity for the p-polarized curves above the critical angle indicates a surface plasmon resonance in the gold film for the different air-gap thicknesses. The small, medium, and large air-gaps used the measurement show the depth of the dip increases as the air-gap thickness decreases, indicating higher coupling efficiency to the surface plasmon resonance.

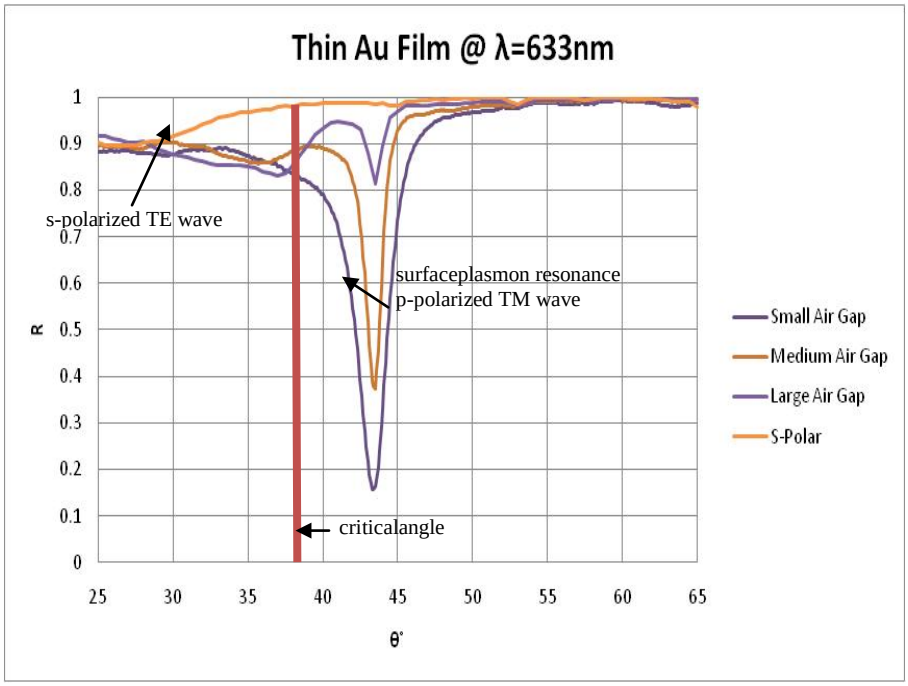

Figure 9. ATR Measurements as a Function of Incident Angle.
A Surface Plasmon Resonance is Observed for P-polarized Light Above the Critical Angle and No Resonance Occurs for the Ss-polarized Light.

The dispersion relation for a continuous gold metal film was determined from the ATR measurements and the results are shown in Figure 10. The dispersion for the plasmon resonance of the gold film is bound by the dispersion of light in free space and the dispersion of the light in the cylindrical-lens, as it should be according to [4].

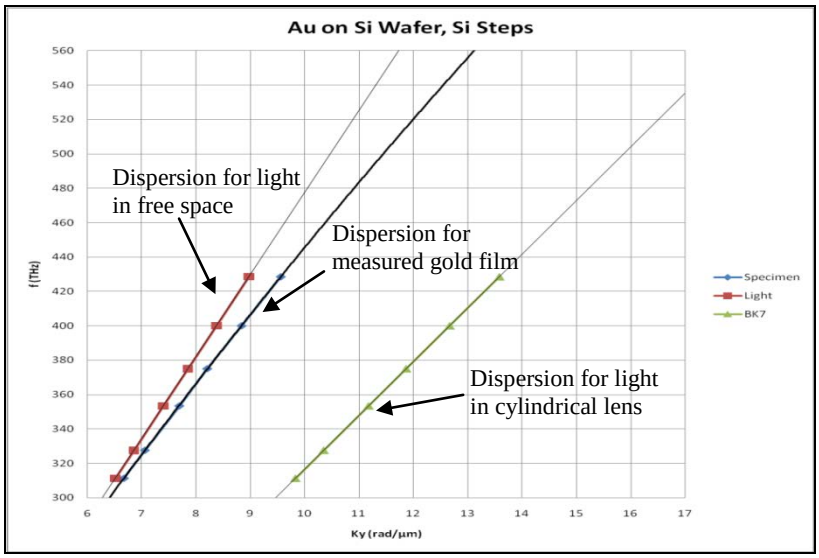

Figure 10. Dispersion of Light in Free Space, Gold Film, and Cylindrical Prism.
*The Dispersion for Light in Free Space is ω = c*k, for Light in the Gold Film is ω = (c*k/(n*sinα)), and for Light in the Cylindrical Lens is ω=c*k/(n).*

We used ATR measurements for a 4-layer nanodot medium to determine it dispersion. The results are shown in Figure 11.

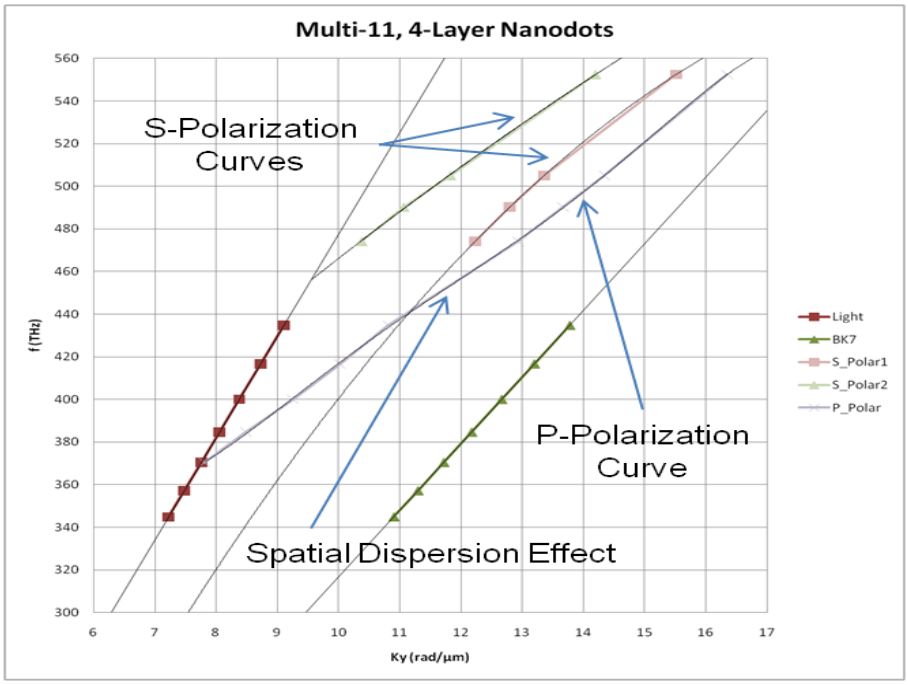

Figure 11. The Dispersion for Light in Free Space Gold Nanodot Media. With S- and P- polarization, Cylindrical Lens, and Polariton Behavior.

The dispersion for the nanodot medium is bound by light in free space and by light in the cylindrical-lens as well. The results in Figure 11 show that the nanodot medium responds to both p- and s- polarization. The dispersion for the p- polarization response has an inflection point at approximately 445 Terra-Hertz (THz). The line shape of the p-polarized dispersion curve indicates that there is a plasmon-polariton [5] response at wavelengths below 445 THz and that above 445 THz no plasmon response is observed. The inflection point in the p-polarized dispersion indicates there is no band gap in the nanodot medium like the band gap that occurs for the plasmon behavior of the gold film.

For magnetic plasmon behavior in a medium, a nanodot inclusion like the one shown in Figure 12 was chosen. The nanodot structure consisted of 4 silver nanospheres arranged in a ring. The nanosphere ring is analogous to SRRs at RF frequencies. The cluster of nanoparticles forming a ring was proposed by Professors Engheta and Alù [6]. Figure 12 shows simulated results of the silver 4-nanoparticle ring obtained from Prof. Engheta. For the simulation, the four silver nanoparticles were suspended in air and results show the nanoparticle ring resonating at 560THz. Since the nanoring in Figure 12 was modeled as four silver nanospheres suspended in air, this nanoring could not be fabricated. The fabrication processes available to us for patterning the nanorings are Ebeam or nanosphere lithography.

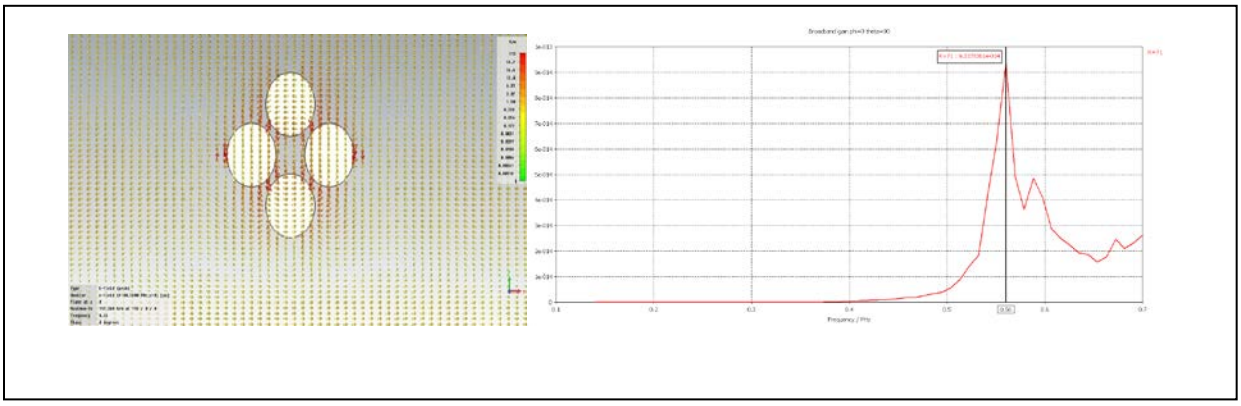

Figure 12. Engheta Initial Design and Analysis.
Left is a 4-element Nano-Sphere Ring (4NSR) and Analysis of H-Field Between Spheres.
Right is H-Field vs. Frequency.

These lithographic processes are planar and require the pattern to be printed on a substrate. This limits the shape of the nanoparticles to cylinders for the Ebeam and a pyramidal shape particle for the nanosphere lithography. The use of the substrate and the change in the shape of the nanoparticles means our nanorings will not behave like the modeled silver nanoparticle ring suspended in air. To confirm the HFSS simulation results of our nanoparticle would with agree with Engheta and Alù's Comsol simulation. We started with Engheta and Alù's 4- sphere nanoring suspended in air and simulated it in HFSS. We modeled the Engheta and Alù's nanoring with silver and gold since we planned to use gold for the initial study. The results from the HFSS simulation are shown below in Figure 13.

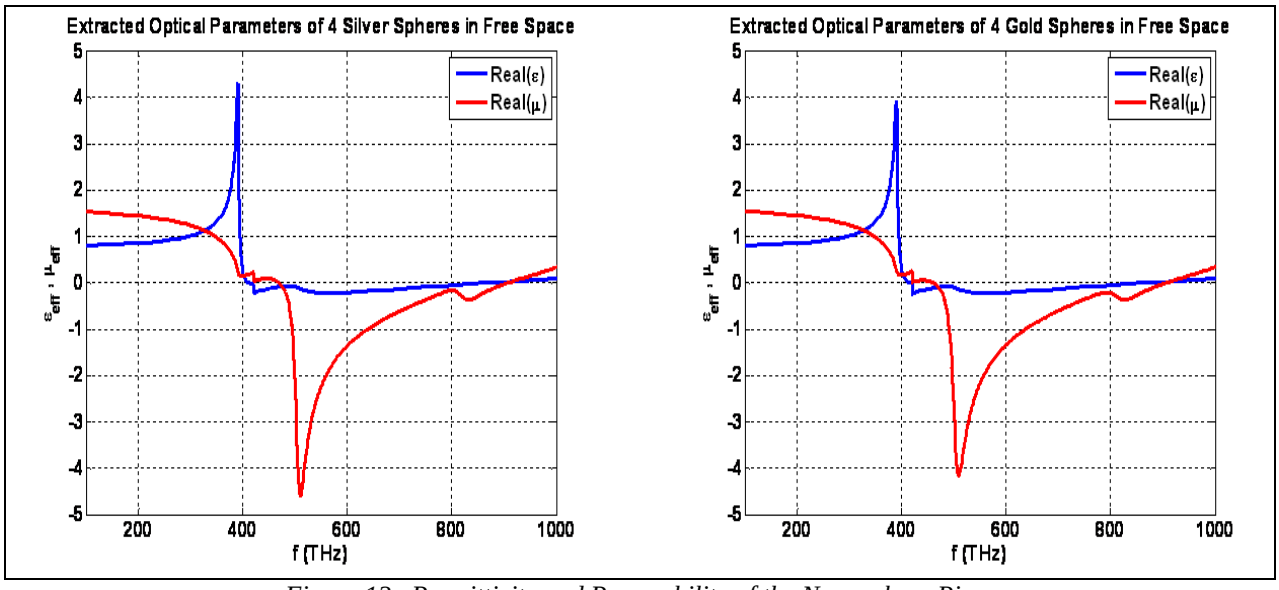

Figure 13. Permittivity and Permeability of the Nanosphere Ring.
Made of (Left) Silver, (Right) Gold.

Figure 13 shows the real part of ε and μ the 4 nanospherering suspended in air for silver and gold as a function of frequency. The real part of μ shows a strong resonance with a negative value at approximately 520 THz, very close to Engheta and Alù's 560THz peak magnetic field resonance.

It also shows it is negative from approximately 500 to 800 THz, which includes the 500-700THz range at which strong magnetic fields are observed in Engheta and Alù's model. Since results of our HFSS simulation matched those of Engheta and Alù, we modeled our four nanocylinder ring suspended in air and on an aluminum oxide substrate in HFSS.

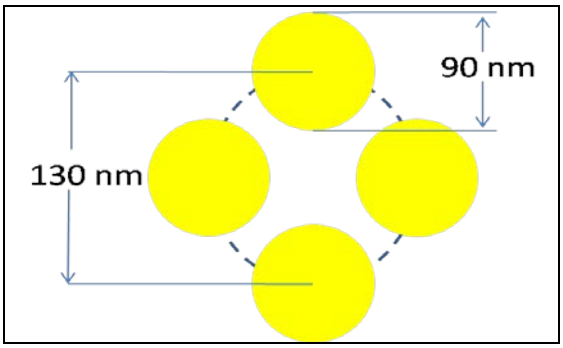

Figure 14. Diagram of the Four 90 nm Diameter Nanocylinders. Centered on a 130 nm Circle to Form the Ring Used for the HFSS Simulations and for the Patterned Ebeam Lithography.

A diagram for the nanoring used in the simulation is shown in Figure 14. The diagram shows four nanocylinders centered around a 130 nm circle. This leaves the spacing between the nanocylinders at 2 nm. The simulated results for the gold nanoring with cylindrical particles suspended in air and on an aluminum oxide substrate are shown in Figure 15 below.

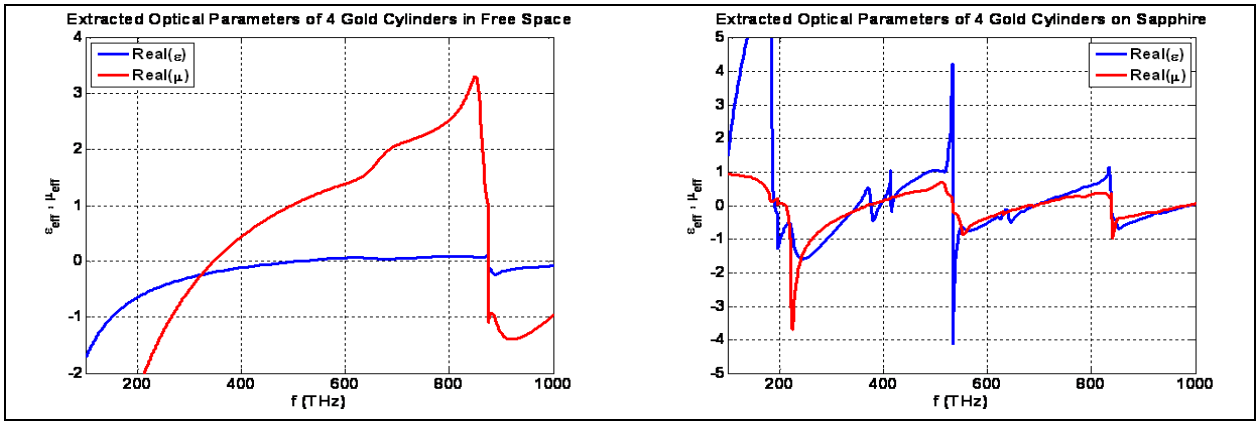

Figure 15. Extracted Permittivity and Permeability of the Gold Nano-Cylinder Ring. In Air (Left), and on a Sapphire Substrate (Right).

The frequency response of the real part of μ for the nanocylinder ring suspended in air shown on the left in Figure 15 is significantly different from the nanosphere ring suspended in air. The resonance in μ for the nanoring with the cylinders suspended in air is about860THz, which is above the resonant frequency of μ for the nanoring with spheres suspended in air (~520THz). The nanocylinder ring on the aluminum oxide substrate shown on the right of Figure 15 has more structure than the nanocylinder ring suspended in air. The nanocylinder ring on aluminum oxide has 3 distinct resonances at approximately 250, 550, and 850THz. Ebeam lithography was used to fabricate an array of nanocylinder rings on an aluminum oxide substrate. The fabricated nanorings are shown in Figure 16. Though Ebeam lithography is precise, the critical dimensions for the nanocylinders are beyond the resolution of the Ebeam lithography system. In Figure 16 one can see the imperfections of the nano-rings for various fabricated nanocylinder and ring diameters.

The imperfections will affect the behavior of the nano-rings.

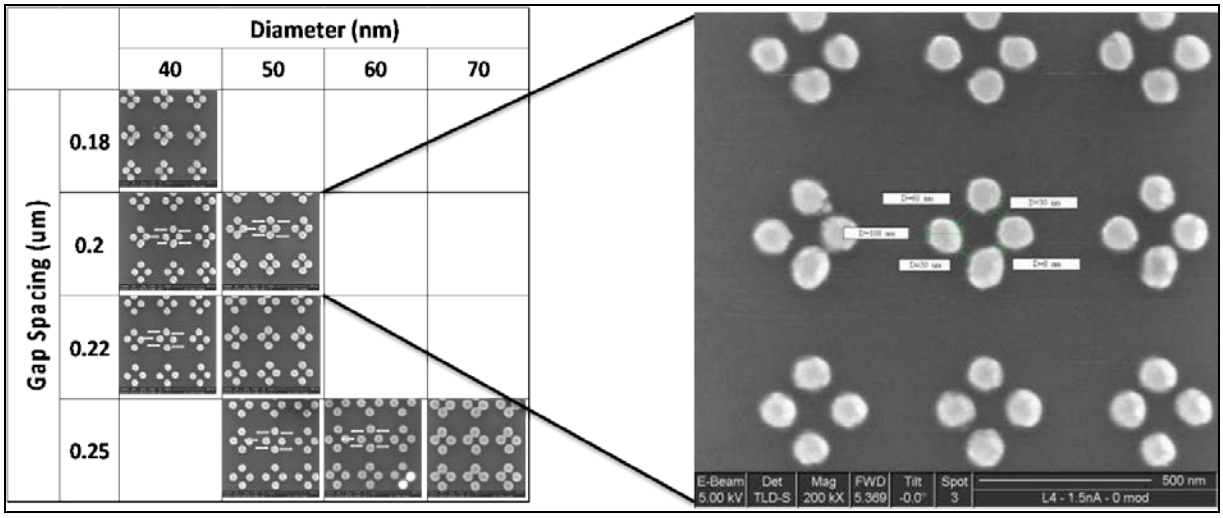

Figure 16. Ebeam Patterned Nano-Ring Made from the Nanocylinders.
The Nanocylinders are Required to 90 nm in Diameter with a 2 nm Spacing between the Cylinders in the Ring.

Figure 16 on the right shows a case where all nanocylinders are resolved but with some variation in the diameter and spacing. To determine the effects of cylinder size and spacing variations of the nanorings, an average value for the cylinder size and spacing was used to simulate the nanoring. The result of the simulation is shown in Figure 17.

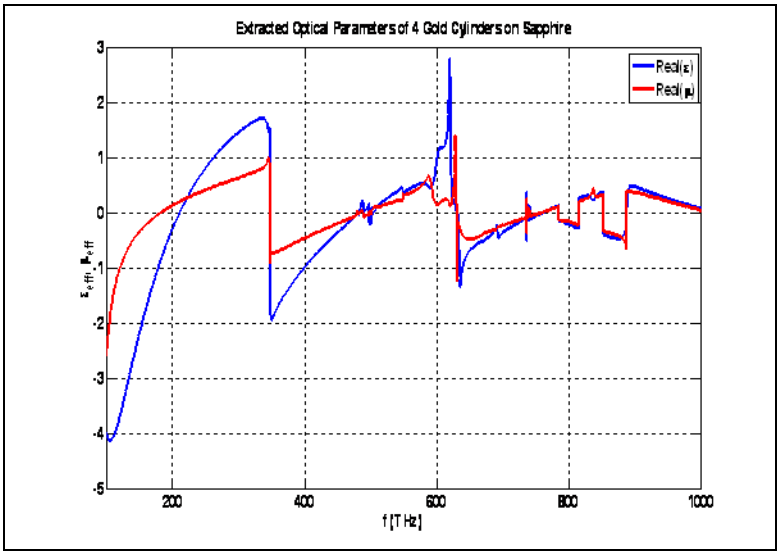

Figure 17. Simulated Results of the Patterned Nanorings.
Using Mean Values for the Cyclinder Diameters and Spacing.

The simulation results shown in Figure 17 show that the first two resonances for the nanocylinder ring have moved down in frequency compared to resonances in Figure 15, as expected since the diameter and spacing has increased. The changes in the resonances observed in Figures 15 and 17 indicate that controlling the diameter and spacing of the nanocylinders in the fabrication process is critical for building optical metamaterials at the desired wavelengths.

We are presently characterizing the nanocylinder rings to determine the resonant frequency of the fabricated four nanocylinder rings and to determine how the size and spacing of the nanocylinders in the ring affect its predicted response compared to its actual response. A series of SRR-WP media are being fabricated to validate the effect of the neighbor to neighbor coupling of the SRR-WP unit cells and the effect of coupling between SRRs and WP.

4.0 References

1. Veselago V.G., *"The Electrodynamics of Substances with Simultaneously Negative Values of ε and μ,"* Soviet Physics USPEKHI, Vol. 10, No. 4, Jan-Feb 1968.
2. Marqués R., Martel J., Mesa F., and Medima F., *"Left-Handed-Media Simulation and Transmission of EM Wave in Subwavelength Spilt-Ring-Resonator-Loaded Metallic Waveguides,"* Phys. Rev. Lett., Vol. 89, No. 18, 28 Oct. 2002.
3. Derov J.S., Turchinetz B.W., Crisman E.E., Drehamn A.J., and Wing R.M., *"Free Space Measurements of Negative Refraction With Varying Angles of Incidence,"* IEEE Microwave and Wireless Components letts., Vol. 15, No. 9 Sept. 2005
4. Otto A., *"Excitation of Nonradiative Surface Plasma Waves in Silver by the Frustrated Total Reflection,"* Zeitschrift für Physik 216, pp. #398-410 , 1968
5. "Polaritons," Proceeding of the FirstTaormina Conference on the Structure of Matter, Taormina, Italy, 1972, ISBN 0-08-017825-1.
6. Alù A., Salandrino A., and Engheta N., *"Negative Effective permeability and Left-Handed Materials at Optical Frequency,"* Opt. Express, Vol. 14, No. 4 pp. 1557-1567, 20 Feb. 2006.

LIST OF ACRONYMS, ABBREVIATIONS, AND SYMBOLS

ACRONYM/SYMBOL	DESCRIPTION
ε	Permittivity
μ	Permeability
Al_2O_3	Aluminum Oxide
ATR	Attenuated Total Reflection
GHz	Giga-Hertz
HFSS	High Frequency Structure Simulator
RF	Radio Frequency
SRR	Split-Ring-Resonator
THz	Terra-Hertz
TM	Transverse Magnetic
TE	Transverse Electric
WP	Wire Post